Eur. Phys. J. D **28**, 79–90 (2004)
DOI: 10.1140/epjd/e2003-00286-2

THE EUROPEAN PHYSICAL JOURNAL D

Experimental assessment of temperature in plasma wall interaction

Application to PE and POM

W. Bussière[1,a], E. Duffour[1], P. André[1], R. Pellet[1], and L. Brunet[2]

[1] Laboratoire Arc Électrique et Plasmas Thermiques (LAEPT), CNRS UMR 6069, Université Blaise Pascal, 24 avenue des Landais, 63177 Aubière Cedex, France
[2] GIAT Industries, route de Guerry, 18000 Bourges, France

Received 9 December 2002 / Received in final form 25 July 2003
Published online 14 October 2003 –

Abstract. The purpose of this paper is to study the temperature evolution during the interaction of a plasma with an insulating wall in polyethylene ($(CH_2)_n$) and polyoxymethylene ($(CH_2O)_n$). The plasma is initiated by means of a capacitor bank discharge in a copper fuse wire. Due to the energy release the ablation of the insulating wall produces some insulating vapours in addition to the copper vapours corresponding to the wire vaporization. Using neutral copper line intensity ratio assuming a Boltzmann distribution we obtain a temperature evolution from ∼11 000 K to ∼24 000 K in the first few hundreds microseconds of the discharge. For later times the copper lines are strongly self-absorbed and make impossible the diagnostic in a spectroscopic way. Hence the temperature is deduced from the comparison between the experimental and calculated electrical conductivity. So for the decrease of the current the temperature evolves from ∼21 000 K down to ∼6 000 K and depends on the plasma density. The results and the reliability of the two methods are discussed.

PACS. 52.25.Kn Thermodynamics of plasmas – 52.70.Kz Optical (ultraviolet, visible, infrared) measurements – 52.80.Wq Discharge in liquids and solids

1 Introduction

For many years many kinds of insulating material have been tested in electric power apparatus designed to interrupt high fault current (H.B.C. fuse and expulsion fuse, SF_6 circuit breaker) [1,2] or designed to produce a plasma source used for various applications (especially powder ignition in electrothermal chemical launchers) [3,4]. The nature and the dimensions of the dielectric material have been fully investigated in order to select the parameters which in the first case dissipate the most possible energy [5,6], and in the second case transfer the most possible energy to a reactive target. The shape of the plasma produced during the discharge is generally imposed by the use of a dielectric material tube which receives the fuse striking wire. The latter points allow some assumptions which are very convenient for the interpretation of the plasma insulator interaction in theoretical [7,8] and experimental works [9,10]. The tested insulating material is chosen according to the final purpose of the device [11,12]: quartz and boric acid in the case of fuses, polymers in the case of SF_6 circuit breakers and electrothermal chemical launchers.

In modelling the calculations are performed for a temperature scale varying in the range from ∼2 000 K up to ∼30 000 K. In this temperature range the main properties of the plasma made of metallic and insulating vapours vary significantly with the temperature [13–15] and with the ratio of metallic to insulating elements [16]. The properties which strongly depend on the temperature are the electrical conductivity, the thermal conductivity and the viscosity. These are clearly linked to the type of material [17].

Therefore the temperature has to be known during the discharge in order to give a coherent interpretation of the plasma wall interaction. To evaluate the temperature we use two methods which are distinct from each other. In thin plasmas the temperature is commonly deduced from the plasma radiation analysis [18]. The spectroscopic way consists in the evaluation of the ratio between two spectral line intensities [19] or between a spectral line and the continuum intensities [20], or directly from one spectral line intensity or continuum intensity when an absolute

[a] e-mail: william.bussiere@laept.univ-bpclermont.fr

calibration is made [21]. These latter methods give a direct measurement of the plasma temperature. Unfortunately the collection of the available radiation is difficult to realize. Thus the spectroscopic method has to be compared with another. The method which consists in evaluating the temperature from the electrical conductivity measurement has been already used in various applications: railgun plasma armature [22], capillary discharges [23,24], wall-stabilised AC arcs [25], and free-burning arcs [26]. This means is an indirect way to measure the temperature. As a matter of fact the electrical conductivity depends strongly on temperature.

Our experimental approach divides into three steps. First step, we examine the influence of the nature of the polymer and the confining geometry on the discharge. The evolutions of the physical and electrical parameters are given, and the experimental and theoretical results are given separately. Second step, we detail the plasma temperature measurement. We use two methods depending on the time interval studied. The temperature is deduced from the neutral metallic lines intensity ratios assuming a Boltzmann distribution for the energy levels at the beginning of the phenomenon. Hence, the temperature is deduced from the electrical conductivity measurement during the cooling of the plasma. Third step, from the temperature measurement and the calculations, we study the plasma density, and the ratio between the metallic and insulating species during the whole phenomenon.

2 Experimental set-up

2.1 Experimental test device

The section view of the test device is shown schematically in Figure 1. The test tube is designed to allow the measurement of the pressure ($\leq$150 bars), the collection of the plasma radiation and to study the influence of the test tube dimensions and material. In this paper we present the study of a test tube with length-to-radius ratio (l/R) equal to 6 and 8 and constituent material being either polyethylene (PE, $(CH_2)_n$) or polyoxymethylene (POM, $(CH_2O)_n$). Its outer diameter is 10 mm and two inner diameters are tested: 5 mm and 7 mm. The two electrodes are made in brass. The dimensions of the POM-expansion chamber are 50 mm in length and 10 mm in diameter. These dimensions have been tested so as to obtain no high pressure gradient between the expansion chamber inside and the test tube inside during the discharge (Sect. 4.2). Furthermore the expansion chamber wall is made to fit laterally onto the sensitive area of the pressure quartz transducers. A clamping support especially designed to avoid the gas leak between the two main parts of the device is added (not shown in Fig. 1).

To initiate the arc a 0.3 mm-diameter copper striking wire is inserted between the two electrodes inside the test tube. To get the same initial conditions a new test tube is used for each test and the two electrodes are frequently replaced. We do not use any specific working gas. The inner tube is full of ambient air at atmospheric pressure before the discharge.

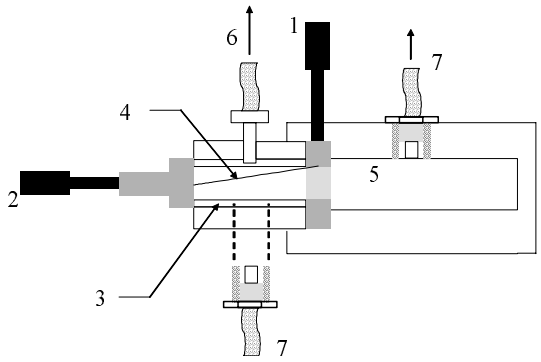

Fig. 1. Diagram of the test device: 1, cathode; 2, anode; 3, insulating test tube (PE, POM); 4, copper fuse wire; 5, expansion chamber; 6, quartz fibre; 7, pressure transducer.

2.2 Energy supply

To provide the energy necessary for the wall ablation a capacitor bank is used. It consists of two sets of seven capacitors (4700 μF each) in series with an inductance of 145 μH. The charge voltage range investigated in this work is included between 220 and 340 V (Tab. 1). So the initial stored energy ranges between 385 J and 925 J. The time lag between the release of the stored energy and the triggering of the measurement devices is of major importance especially for the triggering of the CCD matrix in the streak mode. So it has been tested and adjusted according to the two main influential parameters: the charge voltage and the length-to-radius ratio (l/R) (Tab. 2).

2.3 Diagnostics

2.3.1 Current and voltage measurement

The electric current through and the voltage across the electrodes are measured by means of a 416 $\mathrm{A\,V^{-1}}$ current shunt and a 100 $\mathrm{V\,V^{-1}}$ voltage shunt respectively. These two voltages are displayed on a TEK TDS 224 oscilloscope and the data are monitored by means of a standard commercial video-PC interface hardware.

2.3.2 Pressure measurement

The pressure evolution during the whole duration of the arc is measured using two Kistler 601A quartz pressure transducers. They are set at right angle to the test device axis. To protect and to prevent a direct exposure of the quartz transducer to the very hot plasma, a thin layer of silicon grease is spread on the sensitive area of the transducers. The pressure can be monitored simultaneously at two different points: at the mid-point of the test tube, and at the mid-point of the expansion chamber.

Table 1. Details of the measurements for the two types of confining tubes. The pressure is the absolute pressure.

		Test voltage (V)	220	240	260	280	300	320	340
PE	3.5	Current peak (A)	990	1015	1048	1106	1166	1181	1207
		Current density (A.mm^{-2})	25.7	26.4	27.2	28.7	30.3	30.7	31.4
		Energy (J)	217	250	291	336	390	464	501
		Energy / Volume (10^6 J.m^{-3})	282	325	378	436	506	603	651
		Pressure peak (Bar)	28.3	39.8	46.8	56.8	72.0	82.3	92.8
	2.5	Current peak (A)	998	1048	1065	1065	1130	1131	1182
		Current density (A.mm^{-2})	50.8	53.4	54.2	54.2	57.6	57.6	60.2
		Energy (J)	160	192	216	254	298	311	381
		Energy / Volume (10^6 J.m^{-3})	407	489	550	646	758	791	969
		Pressure peak (Bar)	27.4	35.3	41.2	48.4	55.6	63.8	77.8
POM	3.5	Current peak (A)	974	998	1056	1090	1131	1148	1190
		Current density (A.mm^{-2})	25.3	25.9	27.4	28.3	29.4	29.8	30.9
		Energy (J)	191	229	267	310	353	415	471
		Energy / Volume (10^6 J.m^{-3})	248	297	347	403	458	539	612
		Pressure peak (Bar)	24.6	28.0	35.3	41.3	58.0	59.6	71.0
	2.5	Current peak (A)	940	982	1040	1090	1123	1173	1182
		Current density (A.mm^{-2})	47.9	50.0	53.0	55.5	57.2	59.7	60.2
		Energy (J)	151	177	196	223	253	281	314
		Energy / Volume (10^6 J.m^{-3})	384	450	499	567	644	715	799
		Pressure peak (Bar)	23.4	26.9	32.8	37.1	41.9	49.9	56.8

Table 2. Stored energy-to-total dissipated energy ratio (r) and arc duration (t_a) with the corresponding standard deviations (σ_r, σ_{ta}).

l (mm)	R (mm)	l/R	$r \pm \sigma_r$ (%)		$t_a \pm \sigma_{ta}$ (ms)	
			PE	POM	PE	POM
20	3.5	≈ 6	50.7 ± 1.2	48.2 ± 0.8	2.9 ± 0.1	2.8 ± 0.1
20	2.5	8	38.4 ± 0.8	35.0 ± 1.9	2.2 ± 0.2	2.1 ± 0.1

2.3.3 Radiation analysis

Spectroscopic apparatus

During the discharge the plasma emits a radiation allowing the evaluation of the plasma temperature (Sect. 4.3). The radiation viewing point is located at the mid-point of the insulating test tube. The quartz fibre used to collect the light is inserted through the insulating wall into the close-fitting channel. The channel length is fitted to avoid direct contact between the quartz fibre end and the plasma. Thus the light issued from the plasma is collected by the quartz fibre *via* a weak thickness of the insulating material. Since the radiation emitted is strong and the absorption by the thickness of the optical fibre channel is weak and can be estimated, we obtain a sufficiently high radiation level to perform the spectroscopic analysis. The other end of the quartz fibre is connected to the 80 μm-entrance slit of the spectroscope.

The spectrometer is a Chromex 500IS with a 0.5 m-focal length and equipped with a CCD matrix. We have worked with a 600 line mm^{-1} grating. The corresponding spectral range investigated is [450–540] nm. The size of the CCD matrix is 1242 × 1152 pixels. The set of setting parameters (exposure time and shifting of each track) is fitted according to the duration and the brightness of the phenomenon. We have worked with 60 tracks with a duration of 0.030 ms or 0.050 ms each. An electronic circuit is used to control the start of the power supply and the shifting of the tracks on the CCD matrix.

Relative intensity calibration

The relative intensity calibration of the optical system (spectrometer, CCD matrix, quartz fibre) is carried out using a tungsten ribbon lamp in the spectral range [450–540] nm. As a matter of fact it is necessary to perform a relative intensity calibration for two main reasons. Firstly we have to correct the possible non linear response of our optical acquisition system over the investigated spectral range. Secondly the light emitted by the plasma is absorbed by the weak material thickness of the wall before being collected by the quartz fibre. Thus we measure the decrease in intensity due to the material thickness for the two diameters, that is to say the ratio

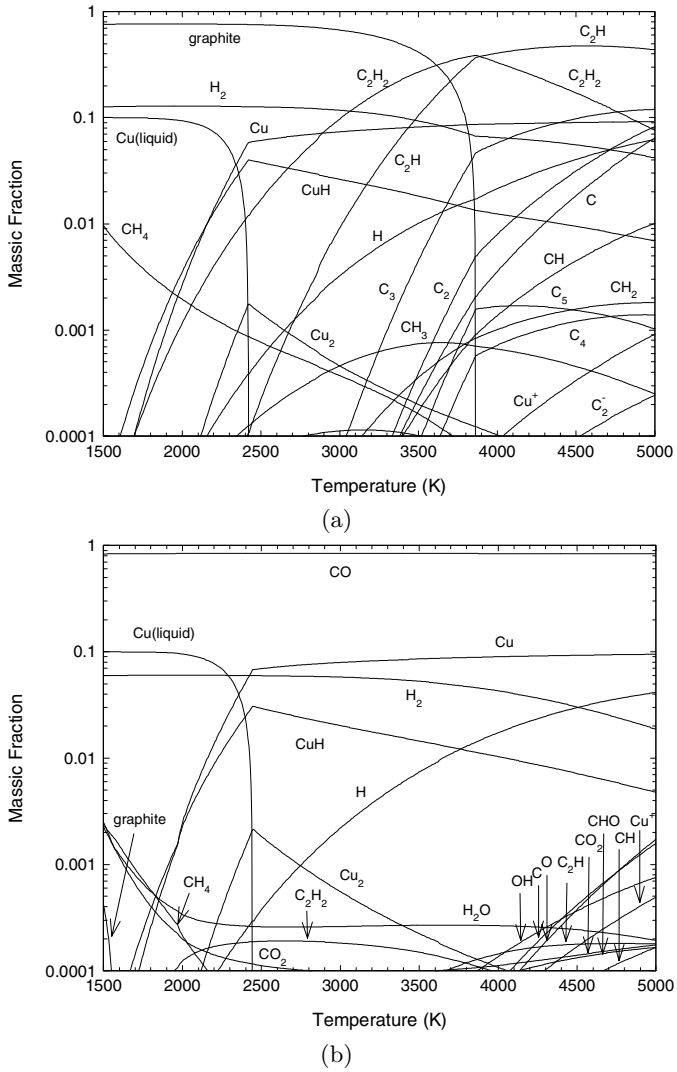

Fig. 2. Massic fraction of chemical species *versus* temperature for a plasma formed of (a): PE and copper (0.45 kg/m^3; 0.05 kg/m^3), (b): POM and copper (0.45 kg/m^3; 0.05 kg/m^3).

$I_\lambda/I_{0,\lambda}$ for the spectral range [450–540] nm ($I_{0,\lambda}$ is the radiation intensity emitted by the tungsten ribbon lamp; I_λ is the collected radiation intensity). Respectively for the 5 and 7 mm-diameters, we obtain $(1.2 \pm 0.5) \times 10^{-2}$ and $(7.8 \pm 1.8) \times 10^{-2}$ for PE, $(3.1 \pm 1.3) \times 10^{-3}$ and $(6.3 \pm 1.1) \times 10^{-3}$ for POM. Of course we observe that the higher the thickness, the higher the absorption. Furthermore for the considered spectral range [450–540] nm, the absorption is higher for POM than for PE.

3 Theoretical calculation

Since the plasma gets a high pressure (up to 100 bars) in the confinement volume, we consider that the plasma is at thermal equilibrium. We assume that the temperature T and the volume V are maintained constant. In these conditions the thermodynamic equilibrium is reached when the total Helmholtz free energy is minimal. In our paper [27] we give the composition, the pressure and the thermodynamic properties calculated for plasma formed in insulator vapours of PC and POM at fixed volume. In the current study we add in our calculation the chemical species due to the copper constituting the fuse wire and apply the calculation for plasmas formed in insulator vapours of PE and POM (Figs. 2a and 2b). So we take into account 18 monoatomic species, C, C^-, C^+, C^{++}, C^{+++}, Cu, Cu^-, Cu^+, Cu^{++}, Cu^{+++}, H, H^-, H^+, O, O^-, O^+, O^{++}, O^{+++}, 21 diatomic species CH, CH^+, CH^-, CO, CO^+, CO^-, C_2, C_2^-, C_2^+, CuO, CuH, Cu_2, OH, OH^+, OH^-, H_2, H_2^+, H_2^-, O_2, O_2^-, O_2^+, 21 polyatomic species C_2H, C_2H_2, C_2H_4, C_2H_4O, C_2O, C_3, C_3O_2, C_4, C_5, CH_2, CH_2O, CH_3, CH_4, CHO, CHO^+, CO_2, CO_2^-, H_2O, H_3O^+, HO_2, O_3 and electrons.

Table 3. Methods used to determine the momentum-transfer cross Q^1 or the average cross-section $\bar{Q}_{1j}^{(1,1)}$.

Species	Dipôle	Method	References
Cu		Numerical Integration	[28-32]
Cu_2		$\bar{Q}_{1Cu_2}^{(1,1)} = \pi^{2/3}\sqrt{2\left(\frac{\bar{Q}_{1Cu}^{(1,1)}}{\pi}\right)^{1.5}}$	
CuO		$\bar{Q}_{1CuO}^{(1,1)} = \pi^{2/3}\sqrt{\left(\frac{\bar{Q}_{1Cu}^{(1,1)}}{\pi}\right)^{1.5} + \left(\frac{\bar{Q}_{1O}^{(1,1)}}{\pi}\right)^{1.5}}$	

The electrical conductivity is given in our paper [16] for several insulator vapours but without copper and at fixed pressure. In Tables 3 and 4 we give the necessary data to complete those given in [16] to calculate the electrical conductivity.

In Figure 4 we show a MEB view of the test tube wall after the discharge and the cooling. We observe the presence of two copper shapes: droplet shape and cluster shape. So we can say that the droplets are formed from the parts of the copper wire that do not have the time to vaporise and that the clusters are formed when the copper becomes part of the plasma and condenses on the wall during the cooling. Thus the exact copper proportion that becomes part of the plasma is difficult to determine. Furthermore, since we use the electrical conductivity and the pressure in the plasma phase to interpret the experimental results, we have to study the influence of copper on these physical properties. From the pressure measurements obtained at the beginning of the discharge and from the number of copper droplets observed, we conclude that the copper percentage involved in the plasma phase is weak. Thus we make the calculation with a W.P. (Weight Percentage) of 10% which is taken as a very high limit. In Figure 3a we show the electrical conductivity for POM and PE with copper *versus* temperature at a fixed density of 0.5 kg/m^3. We observe that with copper the electrical conductivity is higher than with pure insulating. The difference is about a factor of 4 for POM and a factor of 2 for PE at 8 000 K, but becomes lower than a factor of 1.25 for temperature higher than 10 000 K.

Table 4. Coefficients of the fitting of $\bar{Q}_{1j}^{(1,s)}$ available between 1 000 and 30 000 K. These coefficients are used in the relation [33]: $\bar{Q}_{1j}^{(l,s)} = a_1 \ln(T) + a_2 + a_3 T + a_4/T + a_5/T^2 + a_6/T^3 + a_7/T^4$.

j	s	a1	a2	a3	a4	a5	A6	a7
Cu	1	-55.942	541.231	0.0015783	554324	-5.55829e+008	2.04748e+011	-2.74537e+013
Cu	2	-55.9419	522.583	0.0021044	369550	-1.85278e+008	1.24249e+006	9.15093e+012
Cu	3	-55.9421	508.599	0.00263051	277161	-9.26376e+007	-336107	1.11347e+008
Cu	4	-55.9424	497.414	0.00315662	221727	-5.55793e+007	-2.23767e+006	4.6504e+008
Cu	5	-55.9421	488.088	0.00368272	184774	-3.7054e+007	-828981	1.38884e+008
Cu2	1	-88.8019	859.147	0.00250539	879937	-8.82326e+008	3.25018e+011	-4.35803e+013
Cu2	2	-88.8022	829.549	0.00334053	586623	-2.94108e+008	-302296	1.45268e+013
Cu2	3	-88.8025	807.352	0.00417567	439964	-1.47049e+008	-2.8424e+006	5.28881e+008
Cu2	4	-88.8024	789.589	0.0050108	351973	-8.82305e+007	-750673	5.98177e+007
Cu2	5	-88.8022	774.788	0.00584593	293311	-5.88203e+007	-441046	2.31037e+007
CuO	1	-55.6271	538.494	0.00162694	555643	-5.56937e+008	2.05241e+011	-2.7535e+013
CuO	2	-55.627	519.951	0.00216925	370429	-1.85648e+008	1.75569e+006	9.17793e+012
CuO	3	-55.6274	506.047	0.00271157	277820	-9.28225e+007	-28934.6	4.28867e+007
CuO	4	-55.6275	494.923	0.00325389	222255	-5.56918e+007	-1.24693e+006	3.03956e+008
CuO	5	-55.6278	485.654	0.00379621	185209	-3.71231e+007	-3.82296e+006	7.84461e+008

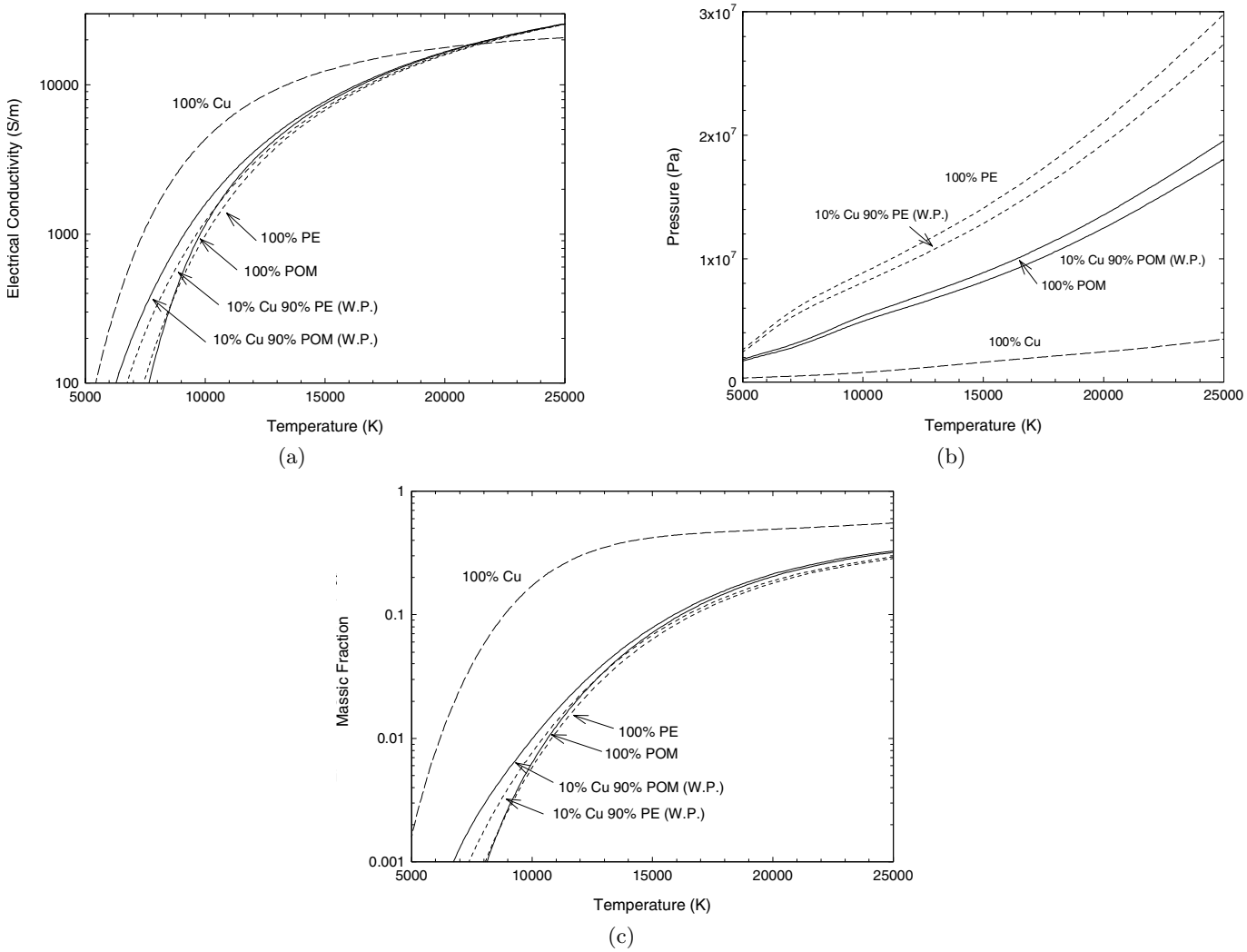

Fig. 3. (a) Electrical conductivity *versus* temperature for several mixtures of PE, POM and Cu (W.P.) and for a density fixed at 0.5 kg/m^3. (b) Pressure *versus* temperature for several mixtures of PE, POM and Cu (W.P.) and for a density fixed at 0.5 kg/m^3. (c) Massic fraction of electrons *versus* temperature for several mixtures of PE, POM and Cu (W.P.) and for a density fixed at 0.5 kg/m^3.

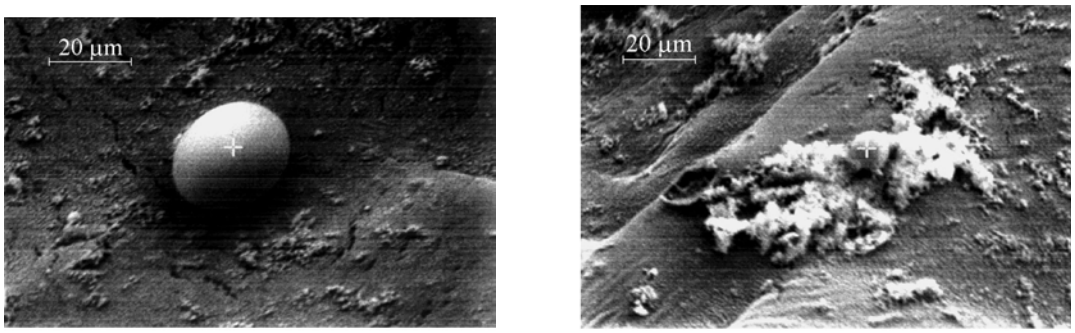

Fig. 4. MEB viewing of a PE test tube after the discharge: (a), copper droplets; (b), copper granular cluster.

In Figures 3b and 3c we show the pressure and the massic fraction of electrons for POM and PE with copper *versus* temperature at a fixed density of 0.5 kg/m^3. We observe that for the same density the pressure is higher with PE than with POM. The influence of copper on pressure is less than 8%. On the contrary the massic fraction of electrons (Fig. 3c) is definitely higher with copper than with insulator vapours. For temperatures higher than 10 000 K the influence of the copper proportion (10% W.P.) for the two polymers is not significant. This justifies partly the discrepancies observed for the electrical conductivity of the various mixtures of PE and POM.

4 Data analysis

The measurement of the current peak, the deduced current density, the total dissipated energy, the volumic energy and the pressure peak are given in Table 1 for the two confining test tubes and the two materials. To deduce the maximum current density and the volumic energy we make three approximations: the radius increase due to the ablation can be neglected, the channel is fully filled by the plasma, and the temperature is the same in the whole of the test tube volume. Thus all the estimations are made with the initial radius value. These approximations are discussed in Section 5.

4.1 Current and voltage characteristics

Typical current and voltage profiles are given for PE and POM in Figures 5a and 5b. The current increases linearly up to the maximal value for a time depending on the stored voltage (Fig. 5c). Hence the current decreases roughly linearly with time. The current density values deduced from the constant radius approximation are in the range [25–60] A mm^{-2}.

At the early beginning of the phenomenon the voltage increases slowly and steadily. There are two rapid changes in the current at times ∼0.754 ms and ∼0.801 ms for POM, and ∼0.773 ms and ∼0.819 ms for PE which correspond to two voltage drops. These moments depend on the stored voltage. The phenomena responsible for the fuse wire breakage are very complex and particularly they markedly depend on the pre-arcing times and the corresponding fault current [34–36]. At this point, in our conditions and to simplify, we can say that until the first of these two drops in the voltage curve (*i.e.* two breaks in current), the fuse wire gradually melts and many copper droplets are produced. The fuse wire is partly vaporised. Once the plasma is initiated ($\gtrsim$0.8 ms) the voltage fluctuates around 360 V. After roughly 2 ms for the two materials there is a gradual and broad voltage drop.

The current peak and the pressure peak vary in a linear way with the charge voltage for the two confining geometries and the two materials. The stored-to-dissipated energy ratio r depends strongly on the l/R value (Tab. 2). The l/R value is thus the main parameter which influences the ability of the device to dissipate the stored energy. On the contrary the material has a weak influence. The mean values and the standard deviations in Table 2 are calculated from the results obtained for the seven charge voltage values. From these values we remark that r is constant for a l/R value and that the discrepancy between the materials is not significant. Such considerations are helpful for the design of the devices, especially for the prediction of the size of the interaction volume and the influence on the electrical conductivity for a given temperature and a given material [37]. From the measurements (Tab. 1) we clearly see two trends: the pressure peak depends on the confining geometry, whereas the current peak is nearly the same for the various confining geometries.

Moreover the calculations (Sect. 3) show that the electrical conductivity is nearly the same for PE and POM for temperatures higher than 10 000 K. This can be seen experimentally in Figure 5d. In fact, for such temperatures, the electrical conductivity depends mainly on the electron concentration (which is very similar for both insulators) and the charged-charged collisions. The latter point is valid for each plasma density put in the calculation.

4.2 Pressure

The pressure evolution *versus* time is showed in Figures 5e and 5f in the case of two typical tests with PE and POM test tubes. All the values are stated in absolute pressure. Two measurements are given: the pressure inside the test tube (curve (1)) and the pressure inside the expansion chamber (curve (2)). The pressure evolution throughout

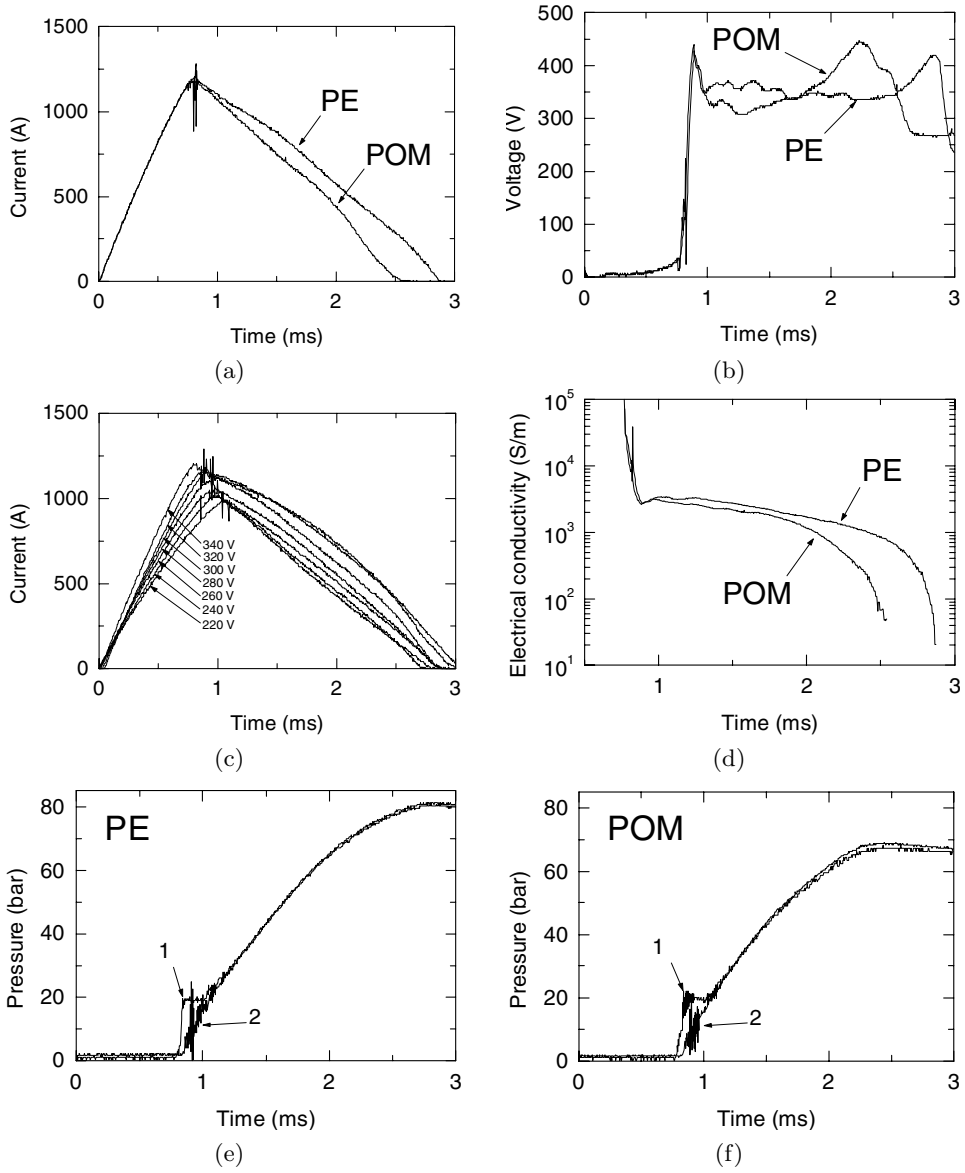

Fig. 5. Typical evolution of: the current (a), the voltage (b), the influence of the stored voltage on the current (c), the electrical conductivity (d), the pressure inside the test tube (curve (1)) and the expansion chamber (curve (2)) *versus* time in the case of a 340 V-stored voltage, for a PE (e) and POM (f)) test tube ($l/R = 8$). The pressure is the absolute pressure.

the whole of the discharge is nearly the same for the two measurements. At the very beginning of the arc (<1.1 ms) the fuse wire disruption generates some pressure peaks which fluctuate very quickly: these correspond to the arc ignition and the induced voltage drops. Once the arc is initiated the material ablation due to the electric energy dissipation is responsible for the more regular pressure increase considering that the temperature is roughly constant during the corresponding time interval (Sect. 5). The maximum pressure values observed are less than 100 bars. After the maximum pressure drop the pressure decreases practically linearly. As a matter of fact, from this moment, the system dissipates more energy than it gains from the electrical supply, which explains the regular pressure decrease.

The discrepancy between the test tube and the expansion chamber trends obtained for the maximum pressure drops is less than 3% which is not significant if we consider the measurement accuracy. On the contrary the two pressure waves are clearly different at the beginning of the phenomenon. The expansion chamber pressure drop is observed 55 μs after the test tube pressure drop. This reproducible time lag for a given set of parameters is quite logical because the pressure wave is propagated over several millimetres before reaching the pressure transducer located at the mid-point of the expansion chamber.

In Figure 6 the pressure peak values *versus* volumic energy are shown. We point out two trends. Firstly, for a given confining geometry the pressure peak value increases regularly with the total dissipated energy. Secondly,

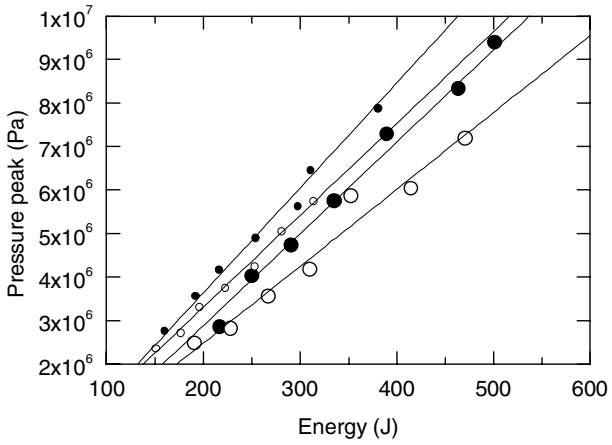

Fig. 6. Pressure peak values *versus* energy. (●) PE, R = 3.5 mm; (•) PE, R = 2.5 mm; (◯) POM, R = 3.5 mm; (∘) POM, R = 2.5 mm.

for a given confining geometry there is no significant discrepancy between the trends observed for the two materials, but the pressure peak values are higher for PE than for POM. The linear trend between the pressure peak and the energy is consistent with the fact that this latter is responsible for the wall ablation.

4.3 Determination of the plasma temperature by means of the spectroscopic method

The plasma temperature is deduced from the ratio of neutral copper line intensity assuming a Boltzmann distribution. Out of the whole spectral range investigated about twenty neutral copper lines have been identified. Most of them cannot be used in the temperature evaluation because the upper energy levels do not differ between them by at least 2 eV [18,38]. The only three neutral copper lines which fulfil the latter condition are commonly used in the temperature evaluation, namely the Cu I 510, 515 and 521 nm whose spectroscopic constants can be found in [39]. Because of the influence of the confinement on the energy release, these three neutral copper lines are strongly self-absorbed on a large time lag during the whole of the radiation emission (Fig. 7). Thus the neutral copper lines can be used only at the early beginning of the phenomenon for which the self-absorption influences the copper line shapes slightly.

From the total intensity of two neutral copper lines quoted 1 and 2 we evaluate the temperature evolution $T(t)$ *versus* time t with:

$$T(t) = \frac{E_{u1} - E_{u2}}{k} \frac{1}{\log\left(\dfrac{g_{u1}\, A_{ul1}\, \lambda_2\, J_2(t)}{g_{u2}\, A_{ul2}\, \lambda_1\, J_1(t)}\right)}$$

where A_{ul} is the transition probability, λ_{ul} is the central wavelength of the neutral copper transition between the levels u and l, g_u is the statistical weight of the upper energy level E_u, and $J(t)$ is the total area of the copper

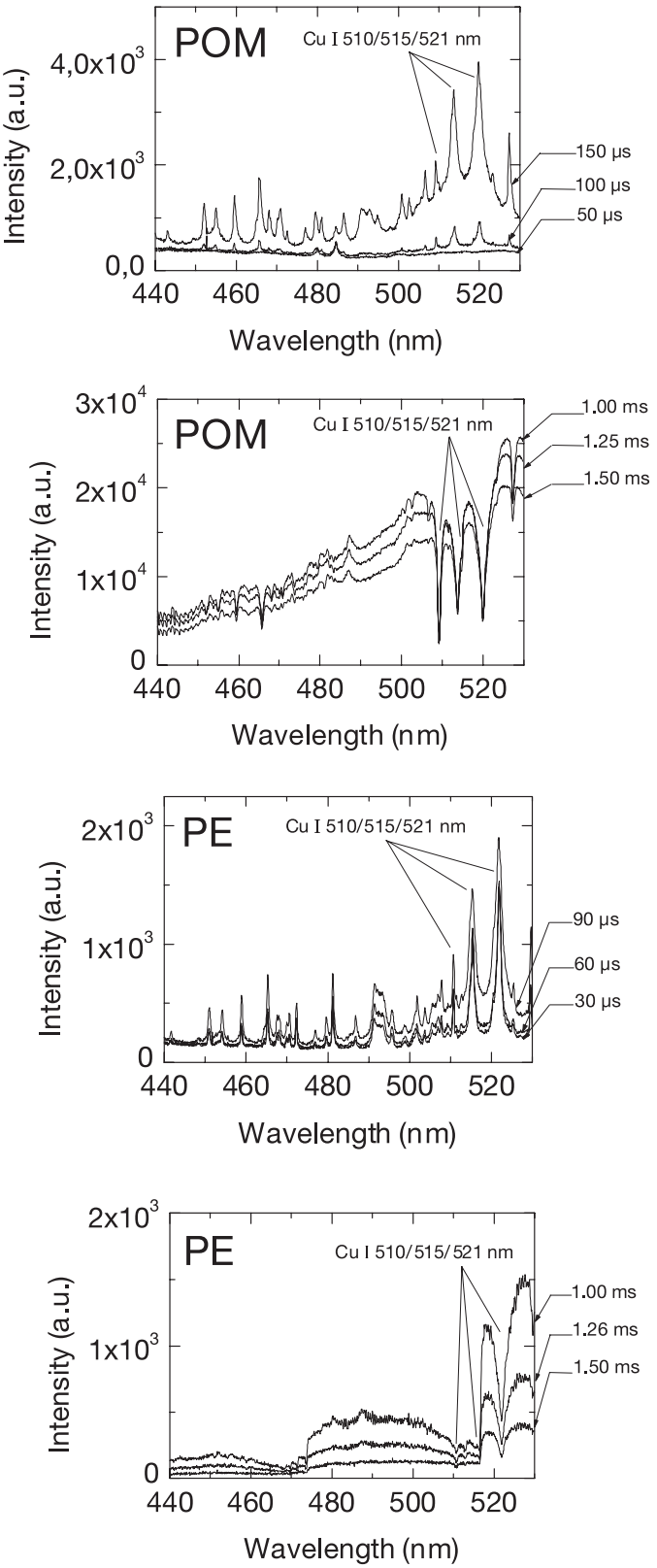

Fig. 7. Plasma radiation in the spectral range [440–530] nm. The time origin corresponds to the arc ignition. The experimental configuration is the same for the two tests (charge voltage, 340 V; inner diameter test tube, 5 mm; total dissipated energy, 464 J and 471 J respectively for PE and POM).

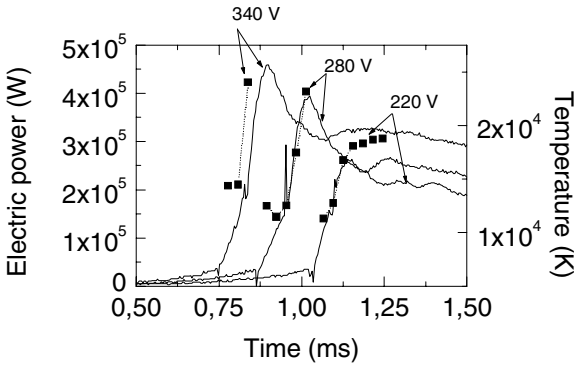

Fig. 8. Evolution of the temperature (■) deduced from the neutral copper lines intensity ratio and the electric power *versus* time for tests performed with a 7 mm-diameter PE test tube.

transitions expressed for the spectra observed during the discharge. This formulation gives the electronic temperature assuming a Boltzmann distribution for the energy levels. Considering that the transitions probabilities are well-known for the neutral copper spectral lines used, the temperature uncertainty $\Delta T(t)$ can be expressed as:

$$\Delta T(t) = \frac{kT^2}{E_{u1} - E_{u2}} \frac{\Delta(J_2(t)/J_1(t))}{J_2(t)/J_1(t)}$$

where $\Delta(J_2(t)/J_1(t))$ is the uncertainty about the experimental intensities.

In Figure 7 we give an example of the spectra observed in the [440–530] nm range at the early beginning of the phenomenon (≈100 μs) and 1 ms after for PE and POM. The origin of the time scale is taken as the arc ignition. The three neutral copper lines used for the temperature evaluation are visible in emission at the very beginning of the time interval studied. Only a few number of spectra are valid for the temperature evaluation.

The results are given in Figure 8 for three different charge voltages in the case of some tests performed with PE. From the spectroscopic measurements we obtain a temperature which increases from ∼10 000 K at the very beginning of the plasma ignition to ∼25 000 K. The temperature increase is observed for a very short time lag about 0.2 ms at the most. The results are only given in the case of PE in so far as no significant discrepancy is found between the two materials by applying the spectroscopic method. For later times the diagnostic based on the spectroscopic method is not valid. In fact the continuous radiation level is very strong and the three neutral copper lines are markedly self-absorbed (Fig. 7). In Table 5 we compare our results with other authors. We obtain similar values of temperature. The discrepancies are coherent if we take into account the input energy, the confining geometry, and the time of the measurement. In our study the main source of error can be attributed to the uncertainty of spectral line intensity, mainly due to absorption. Considering the expression of $\Delta T(t)$ with $\Delta(J_2(t)/J_1(t))/(J_2(t)/J_1(t)) \sim 50\%$ and 25% we obtain respectively $\Delta T(t)/T \sim 36\%$ and 18% at 20 000 K.

5 Study of the electrical conductivity

The electrical conductivity measurement provides the plasma temperature on the condition that the plasma density is known. The plasma density depends on the proportion of metallic elements to insulator vapours.

5.1 Study of the metallic elements to insulator vapours proportion

From the spectroscopic measurements we clearly see that the neutral copper lines are visible in emission for a short time range at the early beginning of the phenomenon. This time range lasts 150 μs at most. Thus to consider the influence of the copper density in the calculation of the plasma properties we have to distinguish two time intervals:

- at the early beginning of the phenomenon: we consider that the plasma is a copper plasma;
- soon after the copper plasma ignition (≈150 μs): we consider that the arc plasma is an insulator plasma.

This assumption for the arc plasma evolution is reinforced by the pressure values obtained at the beginning of the phenomenon. Compared to the pressure levels obtained for the 150 μs-time interval, the values are inferior to 20 bars. Now considering the copper fuse wire used for the plasma ignition, the corresponding mass is about 50×10^{-3} g and it represents an initial copper density of about 66 kg/m^3 for the 7 mm-inner diameter test tube. If we assume that the copper fuse wire is fully vaporized, it should imply some pressure values significantly higher than 100 bars. If we consider a plasma formed with some copper vapours only, and the plasma temperature deduced from the spectroscopic measurement ∼20 000 K, a pressure of about 20 bars after 150 μs would correspond to an initial density lower than 0.5 kg/m^{-3}. This shows that the part of the fuse copper wire which is vaporized is significantly smaller than 1% of the full wire. The latter trend is reinforced by the observation of many copper droplets on the inner area of the expansion chamber (Fig. 4). Moreover the first step in the plasma development seems to be very similar to the depiction of a current-carrying wire submitted to a sudden energy release as it is described in [34]. In fact the main part of the wire disruption appears in the form of the formation of unduloids which are molten parts of the wire. The consecutive arc initiation implies the expulsion of these unduloids or copper droplets. The second step in the plasma development is induced by the plasma-wall interaction and the ablation of the material.

Considering this two-step schema we examine the influence of the copper vapours at the early beginning of the plasma ignition on one side and at the material plasma growth on the other side. During the early 150 μs the arc plasma is treated as a copper plasma. The temperature corresponding to this time range is ∼20 000 K. For such temperatures the electrical conductivity is nearly the same whatever the type of the plasma for a given density (Fig. 3a). Unlike the electrical conductivity the pressure is significantly different in the case of a copper

Table 5. Comparison of the experimental temperatures deduced from various capillary experiments.

Ref.	Type of insulator	Type of experiment	Temperature	Experimental conditions	Diagnosis method	Wavelength (nm)
[40]	Lexan	3 kJ pulsed capillary discharge	23 400 K 16 200 K	time = 30 μs time = 70 μs	Spectroscopy Cu I	510.554, 515.324, 521.820, 529.250, 570.020, 578.213
[41]	Polyethylene	4.5 kJ to 10 kJ capillary discharge	23 210 K 25 760 K	Average plasma temperature	Spectroscopy Cu I	510.55, 515.32, 521.82, 529.25, 570.02, 578.21
[42]	Lexan	1 kJ to 3 kJ capillary discharge	13 925 K 22 050 K	Average plasma temperature (Maximum pressure $\gtrsim$ 100 MPa)	Spectroscopy Cu I Heat flux measurement Electrical conductivity measurement	510.55, 515.32, 521.82, 529.25, 570.02, 578.21
[43]	Polyethylene	80 kJ pulsed capillary discharge	6 960 K 8 120 K	Low pressure (from 13.10^{-6} MPa to 10^{-1} MPa)	Spectroscopy Cu I	510.55, 515.32, 521.82
This work	Polyethylene Polyoxymethylene	Capillary discharge < 1 kJ	~ 14 500 K ~ 24 000 K 13 500 K to 8 500 K 8 000 K to 5 900 K	~ 0.81 ms ~ 0.84 ms ~ 1.2 ms ~ 2.7 ms	Spectroscopy Cu I Electrical conductivity	510.55, 515.32, 521.82

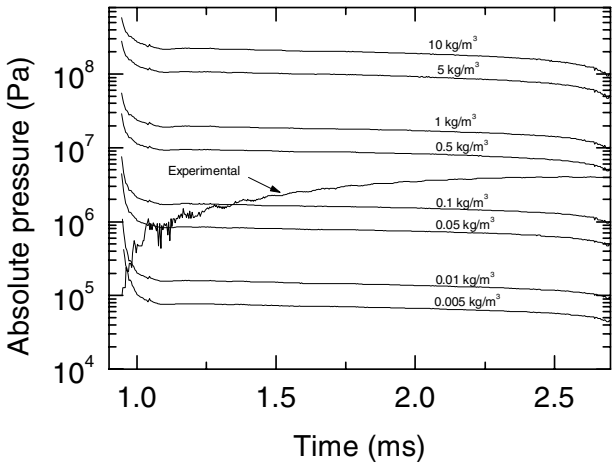

Fig. 9. Evolution of the pressure in the insulator plasma *versus* time in the case of a test with a 7 mm-inner diameter PE test tube. The total dissipated energy is 250 J. The experimental pressure and the pressure calculated for the various densities are absolute values.

plasma (Fig. 3b) for a given density. The values are about 10 times lower than the values obtained for a plasma with insulating vapours only. Once the plasma is initiated ($\approx$150 μs) the plasma is treated as an insulator plasma. The corresponding temperature decreases from $\sim$11 500 K to $\sim$8 000–5 500 K at the end of the discharge. For this temperature range the electrical conductivity and the pressure mainly depend on the material density value. During the cooling of the plasma the calculation shows that the massic fraction of CuO varies between 10^{-5} and 10^{-7} at the most in the case of POM. Thus it can be neglected.

5.2 Experimental assessment of the plasma density

To obtain the plasma density we use the pressure measurements. In Figure 9 we compare the experimental pressure with the calculated pressure in the case of a test performed with a 7 mm-inner diameter test tube and a 240 V-charge voltage. For the time interval [0.95–1.25] ms, the pressure increases up to about 2×10^6 Pa. Due to the gradual energy release and the induced ablation of the wall material, the density of the material plasma is continuously modified. Thus it is not possible to describe the plasma-wall interaction by only one calculation, but by a set of calculations taking into consideration the ablation of the wall and the gradual cooling of the material plasma. This series of the different plasma states is visible in Figure 9 where the experimental pressure is compared with the calculated pressure obtained by taking into consideration the experimental temperature. In fact, especially at the beginning of the discharge, the changes occur very quickly. Taking into consideration the evolution of the experimental curve of the pressure, we clearly see that the material plasma pressure is successively described by some increasing initial densities, namely 0.005 kg/m^3, 0.01 kg/m^3, 0.05 kg/m^3, and 0.1 kg/m^3. After 2 ms the pressure increase is not significant any more, and the curve of the experimental pressure trends to the calculated pressure deduced for an initial density somewhat less than 0.5 kg/m^3.

5.3 Temperature deduced from electrical conductivity

The plasma electrical conductivity σ is deduced from the current i and voltage u measurements assuming that the material plasma completely fills the confining test tube of radius R at the same temperature. Thus it is possible to express the electrical conductivity as:

$$\sigma = \frac{i}{u}\frac{l}{\pi R^2}$$

where l is the length of the confining test tube. This classical formula has been used in strongly flowing cascaded plasma arc plasma [20] assuming a homogeneous current distribution over the arc channel cross-section. In our experiment we take the plasma radius equal to the inner diameter of the test tube. As a matter of fact the total ablated mass is low [11]. The radius increase does not exceed 6% and the ablation is the same along the whole length of the tube [5,7]. Furthermore the radial profile of temperature is given nearly constant over the full radius of the plasma [21]. In capillary discharges the measured voltage U is written as [23,24]: $U = iR_\Omega + L\mathrm{d}i/\mathrm{d}t + i\mathrm{d}L/\mathrm{d}t$, where iR_Ω is the resistive component used to calculate σ, and $L\mathrm{d}i/\mathrm{d}t + i\mathrm{d}L/\mathrm{d}t$ is the inductive component taking

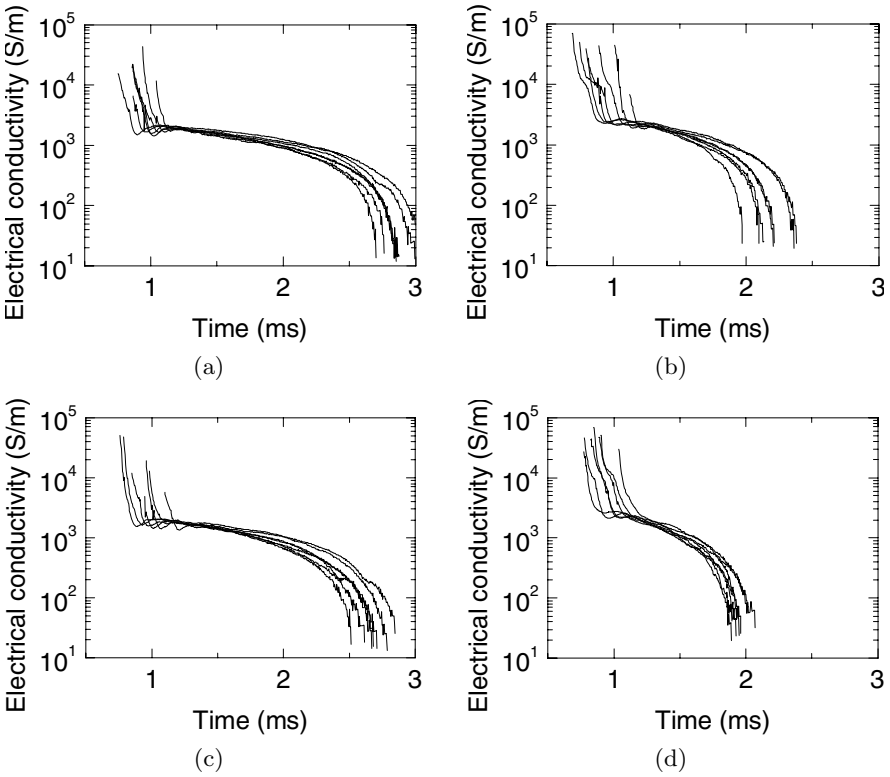

Fig. 10. Evolution of the electrical conductivity *versus* time for PE ((a), R = 3.5 mm; (b), R = 2.5 mm) and POM ((c), R = 3.5 mm; (d), R = 2.5 mm), deduced from $\sigma(t) = (i(t)/u(t))\left(l/\pi R^2\right)$. The curves correspond to the various stored voltages.

into account the change in inductance. The term $i\mathrm{d}L/\mathrm{d}t$ is linked to the change in diameter corresponding to the change from the diameter of the wire to that of the test tube. Once the wire is vaporized, it is negligible. The term $L\mathrm{d}i/\mathrm{d}t$ is the inductance of the current column plus electrodes. $\mathrm{d}i/\mathrm{d}t$ is calculated as the derivative of the current measurement. L is calculated from $U = L\mathrm{d}i/\mathrm{d}t$ at the early beginning of the discharge when the product iR_Ω can be neglected. The maximum value of $L\mathrm{d}i/\mathrm{d}t$ is lower than 10 V. Thus this term is neglected.

In Figure 5d we give a representative evolution of the electrical conductivity *versus* time. From the various experiments given in Figure 10 we notice that the electrical conductivity observed at the very beginning of the phenomenon fluctuates and does not depend on the stored voltage. These fluctuations are linked to the copper fuse wire disruption [35]. The maximum electrical conductivities are overall the same: about 10^3 S/m to 10^5 S/m. Once the material plasma is established, the electrical conductivity decreases slowly with time and the values are in the interval $[0.1\text{–}2.0]\times10^3$ S/m. At the end of the discharge which corresponds to ∼3 ms and ∼2 ms respectively for the 7 mm and 5 mm-diameters, the electrical conductivity decreases quickly down to values about 10^1 S/m. From the measurements we observe that there is no significant discrepancy in the shape of the curves obtained for the two tested materials and that the values lower than 10^2 S/m are observed more rapidly with POM than with PE. In fact the duration of the plasma obtained with POM is shorter.

The electrical conductivity calculation has been performed for eight initial plasma densities ranging from 0.005 kg m^{-3} to 10 kg m^{-3}. Then the evolution of temperature can be deduced. In Figure 11 we give the temperature evolution for a test performed with PE. At the early beginning of the plasma ignition the values range from ∼10 000 K to above ∼21 000 K depending on the plasma density. The trends obtained for the various densities quickly decrease: at 1.2 ms the values spread in the range ∼[13 500–8 500] K, the temperature increasing with the plasma density. For the time interval [1.2–2.7] ms the temperature decreases regularly until the end of the phenomenon. For the end of the discharge, the temperatures range from 5 900 K to 8 000 K.

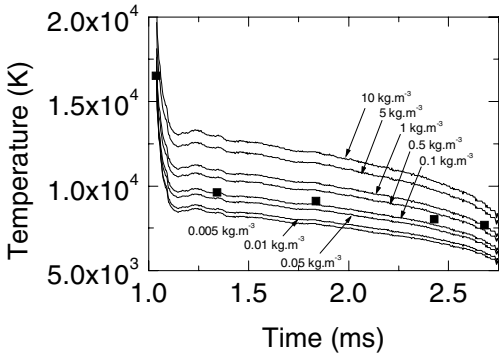

Fig. 11. Temperature *versus* time deduced from the electrical conductivity measurement. The curves correspond to the initial densities ranging from 0.005 kg m^{-3} to 10 kg m^{-3} for a test performed with a 7 mm-diameter PE test tube, 220 V-charge voltage. The points (■) correspond to the intermediate densities.

6 Conclusion

The plasma insulator interaction is used in various industrial devices. Many complex physical and chemical processes such as insulator wall ablation, plasma diffusion, plasma cooling, ... take part during the interaction. One of the parameters to characterize these processes is the plasma temperature. Unfortunately the evaluation of the temperature *versus* time is difficult to obtain. In this paper we have proposed two methods to evaluate it in the case of a capacitor bank discharge in PE and POM tubes. We have described the experimental set-up. Then we have depicted the first method based on atomic spectral lines, and the second method based on the electrical conductivity. We have also discussed the difficulties in their applications and showed that we have found similar results with the both methods in a specific time range. After showing that each method is available in a given time range, we have obtained interesting results. That is to say, for the first hundreds microseconds of the plasma the temperature evolves from ∼10 000 K up to ∼20 000 K. At the decrease of the current, the temperature quickly evolves from ∼20 000 K down to ∼12 500 K, and then more slowly down to ∼6 000 K. We have observed that the lower the diameter, the lower the discharge duration. We have also observed that with POM the discharge duration is lower than with PE. So the time profile of the temperature is the same for all the considered cases, but for different time scales.

References

1. M.A. Saqib, A.D. Stokes, Characteristics of fuse arcing in different fillers, in *Proceedings of the 6th Int. Conf. on Electric Fuses and their Applications*, Torino, Italy, 1999, p. 275
2. A. Wolny, A.D. Stokes, IEE Proc. Gener. Transm. Distrib. **141**(4), 263 (1994)
3. J.M. Lombard, L. Brunet, P. André, E. Duffour, A. Lefort, B. Baschung, *Éléments de modélisation des interactions plasma-matière dans un lanceur électrothermique*, Axes 2, 13 ISL, Saint Louis, mars 1999
4. J.M. Lombard, B. Baschung, D. Grune, A. Carrière, P. André, Analysis of ETC or classical manometric closed vessel tests with coupling of thermodynamic equilibrium calculations: combustion rate, energy losses, *19th Int. Symp. of Ballistics*, 7-11 May, Interlaken, Switzerland, 2001, p. 171
5. A.D. Stokes, L.J. Cao, J. Phys. D: Appl. Phys. **22**, 1697 (1989)
6. J.D. Yan, W.B. Hall, M.T.C. Fang, J. Phys. D: Appl. Phys. **33**, 1070 (2000)
7. EZ. Ibrahim, J. Phys. D: Appl. Phys. **13**, 2045 (1980)
8. L. Muller, J. Phys. D: Appl. Phys. **26**, 1253 (1993)
9. L.J. Cao, A.D. Stokes, J. Phys. D: Appl. Phys. **24**, 1557 (1991)
10. L.J. Cao, A.D. Stokes, J. Phys. D: Appl. Phys. **25**, 669 (1992)
11. P. André, W. Bussière, E. Duffour, L. Brunet, J.M. Lombard, IEEE Trans. Magn. **39**(1), 197 (2003)
12. B. Cheminat, Phys. Appl. **24**, 277 (1989)
13. C.B. Ruchti, L. Niemeyer, IEEE Trans. Plasma Sci. **PS14**(4), 423 (1986)
14. A.B. Murphy, Phys. Rev. E **48**, 3594 (1993)
15. A.B. Murphy, C.J. Arundell, Plasma Chem. Plasma Process. **14**, 451 (1994)
16. P. André, L. Brunet, W. Bussière, J. Caillard, J.M. Lombard, J.P. Picard, Eur. Phys. J. Appl. Phys. (to be published)
17. Z. Koalaga, thèse d'université, Université Blaise Pascal, Clermont-Ferrand, France, 1991
18. W. Lochte-Holtgreven, *Evaluation of plasma parameters, Plasma Diagnostics* (North-Holland Publishing Company, Amsterdam, 1968), Chap. 3, p. 135
19. J. Caillard, C. De Izarra, L. Brunet, O. Vallée, P. Gillard, IEEE Trans. Magn. **39**(1), 212 (2003)
20. J.J. Beulens, M.J. de Graaf, D.C. Schram, Plasma Source Sci. Technol. **2**, 180 (1993)
21. W. Hermann, U. Kogelschatz, K. Ragaller, E. Schade, J. Phys. D: Appl. Phys. **7**, 607 (1974)
22. V. Kowalenko, G.A. Clark, J. Phys. D: Appl. Phys. **33**, 230 (2000)
23. A.W. DeSilva, H.J. Kunze, Phys. Rev. E **49**, 4448 (1994)
24. A.W. DeSilva, J.D. Katsouros, Phys. Rev. E **57**, 5945 (1998)
25. P. Kovitya, S.W. Simpson, J. Phys. D: Appl. Phys. **17**, 1829 (1984)
26. P. Kovitya, J.J. Lowke, J. Phys. D: Appl. Phys. **18**, 53 (1985)
27. P. André, L. Brunet, E. Duffour, J.M. Lombard, Eur. Phys. J. Appl. Phys. **17**, 53 (2002)
28. Y. Itikawa, M. Hayashi, A. Ichimura, K. Onda, K. Sakimoto, K. Takayanagi, J. Phys. Chem. Ref. Data **15**(5), 985 (1986)
29. S. Trajmar, W. Williams, S.K. Srivastava, J. Phys. B. Molec. Phys. **10**(16) 3323 (1977)
30. A.Z. Msezane, R.J.W. Henry, Phys. Rev. A **33**, 1631 (1986)
31. B. Chervy, O. Dupont, A. Gleizes, P. Krenek, J. Phys. D: Appl. Phys. **28**, 2060 (1995)
32. K.F. Scheibner, A.U. Hazi, R.J.W. Henry, Phys. Rev. A **35**, 4869 (1987)
33. J. Aubreton, thèse d'état, Limoges, France, 1985
34. R.E. Brown, P.M. McEwan, Undoloid formation and causation of current interruption in current-carrying wires, in *Proceedings of the 6th Int. Conf. on Electric Fuses and their Applications*, Torino, Italy, 1999, p. 101
35. P. Graneau, J. Appl. Phys. **53**(10), 6648 (1982)
36. A. Wolny, Effect of fuse element confinement on the rate of rise of fuse arc ignition voltage, in *Proceedings of the 6th Int. Conf. on Electric Fuses and their Applications*, Torino, Italy, 1999, p. 135
37. P. André, L. Brunet, IEEE Transact. Plasma Sci. **29**(1), 19 (2001)
38. B. Cheminat, Thèse, Université Blaise Pascal, Clermont-Ferrand, 1983
39. *CRC Hanbook of Chemistry and Physics*, 81th edn. (CRC Press inc., 2001)
40. J. Kohel, L.K. Su, N.T. Clemens, P.L. Varghese, IEEE Trans. Magn. **35**(1), 201 (1999)
41. B. Li, H. Li, Discussion on emission spectroscopy measurements from a dense electrothermal launcher plasma, in *Proceedings of the 19th Int. Symp. of Ballistics*, May 2001, Interlaken, Switzerland, IB24, p. 203
42. O.E. Hankins, M.A. Bourham, J. Earnhart, J.G. Gilligan, IEEE Trans. Magn. **29**(1), 1158 (1993)
43. T. Sueda, S. Katsuki, H. Akiyama IEEE Trans. Magn. **33**(1), 334 (1997)